Available online at www.sciencedirect.com
ScienceDirect
Journal of the European Ceramic Society 26 (2006) 3725–3732
www.elsevier.com/locate/jeurceramsoc

# Phase diagram of the $Al_2O_3$–$ZrO_2$–$Nd_2O_3$ system

S.M. Lakiza *, L.M. Lopato

*Frantsevich Institute for Problems of Materials Science, Krzizanovsky 3, 03142 Kyiv, Ukraine*

Received 29 April 2005; received in revised form 20 November 2005; accepted 3 December 2005
Available online 30 January 2006

**Abstract**

The phase diagram of the $Al_2O_3$–$ZrO_2$–$Nd_2O_3$ system was constructed in the temperature range 1250–2800 °C. The liquidus surface of the phase diagram reflects the preferentially eutectic interaction in the system. Two new ternary and one new binary eutectics were found. The minimum melting temperature is 1675 °C and it corresponds to the ternary eutectic $Nd_2O_3{\cdot}11Al_2O_3$ + F-$ZrO_2$ + $NdAlO_3$. The solidus surface projection and the schematic of the alloy crystallization path confirm the preferentially congruent character of phase interaction in the ternary system. The polythermal sections present the complete phase diagram of the $Al_2O_3$–$ZrO_2$–$Nd_2O_3$ system. No ternary compounds or regions of remarkable solid solution were found in the components or binaries in this ternary system.


*Keywords:* Phase diagram; $Al_2O_3$; $ZrO_2$; β-$Al_2O_3$; $Nd_2O_3$

## 1. Introduction

The $Al_2O_3$–$ZrO_2$–$Nd_2O_3$ system is interesting from the point of obtaining structural and functional high-temperature ceramic materials. Neodymia is one of the effective zirconia stabilizers.[1] Alumina improves thermomechanical properties of $ZrO_2$-based ceramics and improves their hydrothermal stability.[2–4]

The phase diagrams of the bounding binary systems have been examined in some detail.[5–17] The $Al_2O_3$–$ZrO_2$ system is of the eutectic type and is described elsewhere.[5] The $Al_2O_3$–$Nd_2O_3$ system[6–13] includes two compounds: congruently melting at 2090 °C $NdAlO_3$ (NA) with perovskite-like structure and incongruently melting at 1759 °C $Nd_2O_3{\cdot}11Al_2O_3$ (β-phase) with hexagonal β-$Al_2O_3$-type structure. The third incongruently melting at 1905 °C compound $Nd_4Al_2O_9$ was detected but it was discovered to be metastable.[13] No appreciable solubility regions on the base of the components and binary compounds were found in the $Al_2O_3$–$Nd_2O_3$ system. The phase transformations of $Nd_2O_3$ X ⇆ H ⇆ A (where A, H, X—phases on the base of $Nd_2O_3$ with low-temperature hexagonal (A), high-temperature hexagonal (H), high-temperature cubic (X) structures of rare-earths oxides) display on the liquidus as metatectic points at 2200 °C, 93 mol% $Nd_2O_3$ and 2100 °C, 88 mol% $Nd_2O_3$. Two eutectics were detected in the system: β + NA at 1720 °C, 23 mol% $Nd_2O_3$ and NA + $Nd_2O_3$ at 1850 °C, 75 mol% $Nd_2O_3$. The system $ZrO_2$–$Nd_2O_3$ investigated in the 1400–2700 °C range is one of the eutectic type with eutectic coordinates 2115 °C, 70 mol% $Nd_2O_3$.[1,14–17] Wide ranges of solid solutions with fluorite-like F and tetragonal T structures on the base of $ZrO_2$ were found in the system. Solubility on the base of $Nd_2O_3$ does not exceed 20 mol% $ZrO_2$ at the eutectic temperature and decreases up to 5 mol% at 1400 °C. A compound $Nd_2Zr_2O_7$ ($NZ_2$) of a pyrochlore-type structure was found in the F solid solution field below 2220 °C having quite wide temperature dependent homogeneity area.[15,17] The phase transformations of $ZrO_2$ F ⇆ T ⇆ M (where F, T and M—cubic fluorite-like, tetragonal and monoclinic structures of $ZrO_2$ with different $Nd_2O_3$ content) take place in the solid state and are not seen on the liquidus curves. The nature of these transformations is eutectoid.

Systematic information about the interaction character in the system $Al_2O_3$–$ZrO_2$–$Nd_2O_3$ is absent in the literature. In ref.[18] single alloys in $ZrO_2$-rich area of the ternary system were investigated. It was determined that alloy containing 12 mol% $Nd_2O_3$ and 10 mol% $Al_2O_3$ after heat treatment at 1750 °C contains F- and β-phases, the interaction occurs in the presence of some liquid.

In this investigation the $Al_2O_3$–$ZrO_2$–$Nd_2O_3$ phase diagram is presented as isothermal sections at 1250 and 1650 °C, liquidus and solidus projections on the concentration triangle, phase dia-

* Corresponding author. Tel.: +38 44 424 35 73; fax: +38 44 424 21 31.
*E-mail address:* sergij_lakiza@ukr.net (S.M. Lakiza).

0955-2219/$ – see front matter © 2005 Elsevier Ltd. All rights reserved.
doi:10.1016/j.jeurceramsoc.2005.12.005

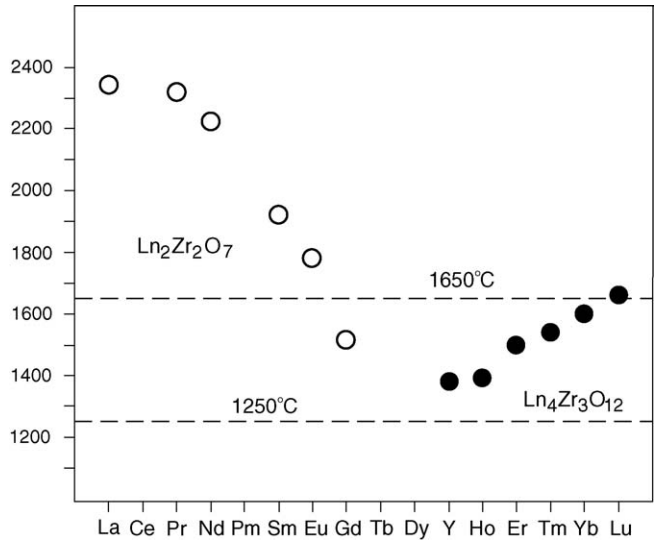


Fig. 1. Temperature stability interval for the superstructures $Ln_2Zr_2O_7$ and $Ln_4Zr_3O_{12}$ in the bounding binary systems $ZrO_2$–$Ln_2O_3$, where Ln—lanthanoids [19].

grams of the triangulating sections, schematic of the reactions proceeding during equilibrium crystallization of melted samples and three isopleths in a wide range of temperatures and concentrations. The temperatures of isothermal sections were chosen according to the temperature stability intervals for the superstructures $Ln_2Zr_2O_7$ and $Ln_4Zr_3O_{12}$ in the bounding binary systems $ZrO_2$–$Ln_2O_3$, where Ln—lanthanoids. The upper temperature stability limits for these superstructures depending on the atomic lanthanoid number are presented in Fig. 1.[19]

The analysis of interaction in the $Al_2O_3$–$ZrO_2$–$Y_2O_3$,[5] $Al_2O_3$–$ZrO_2$–$La_2O_3$[20] systems and the structure of bounding binary systems allowed to assume that the interaction in the system $Al_2O_3$–$ZrO_2$–$Nd_2O_3$ should be determined by the structure of bounding systems in the absence of ternary compounds and appreciable solubility areas. In this case the interaction in the ternary system consists in equilibria of binary compounds NA and β from the bounding system $Al_2O_3$–$Nd_2O_3$ with solid solutions F and superstructure $NZ_2$ from the bounding system $ZrO_2$–$Nd_2O_3$.

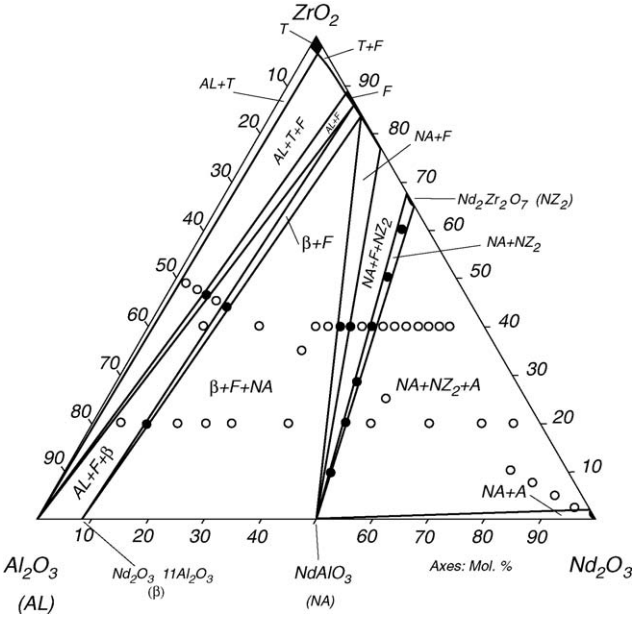


Fig. 2. Isothermal section of the $Al_2O_3$–$ZrO_2$–$Nd_2O_3$ phase diagram at 1250 °C: (●) two-phase samples; (◯) three-phase samples.

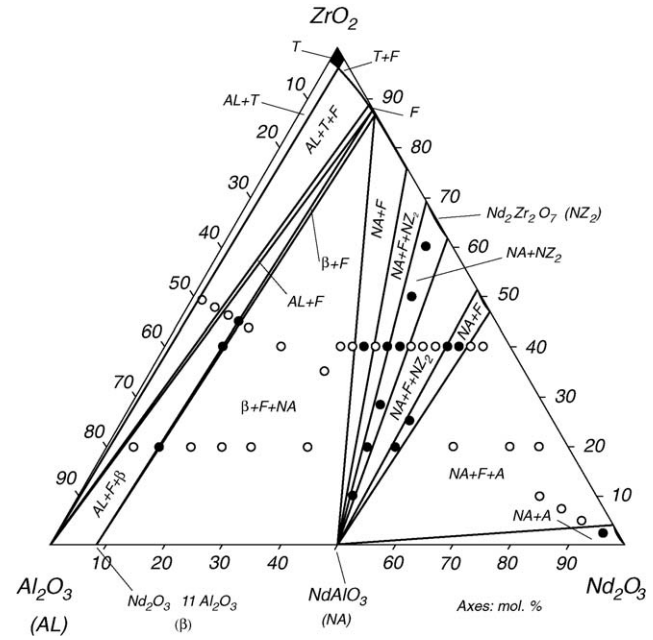


Fig. 3. Isothermal section of the $Al_2O_3$–$ZrO_2$–$Nd_2O_3$ phase diagram at 1650 °C: (●) two-phase samples; (◯) three-phase samples.

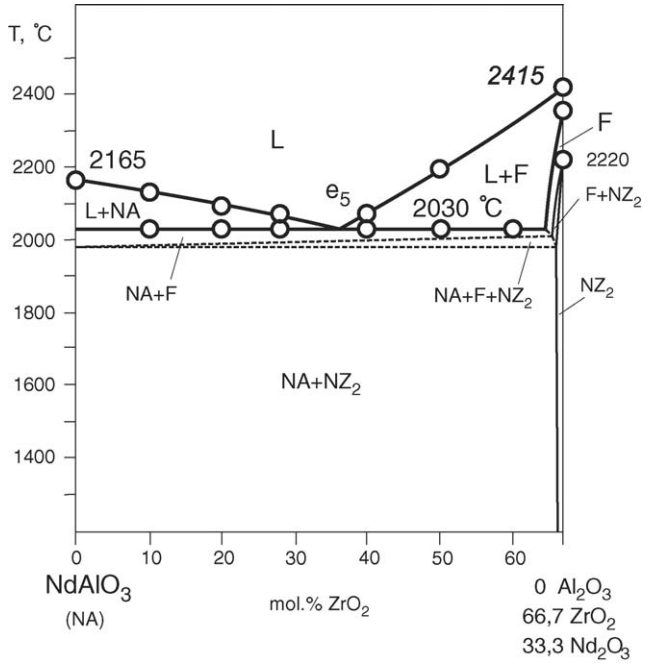


Fig. 4. Partially quazibinary section NA–(66.7% $ZrO_2$–33.3% $Nd_2O_3$) of the $Al_2O_3$–$ZrO_2$–$Nd_2O_3$ phase diagram.

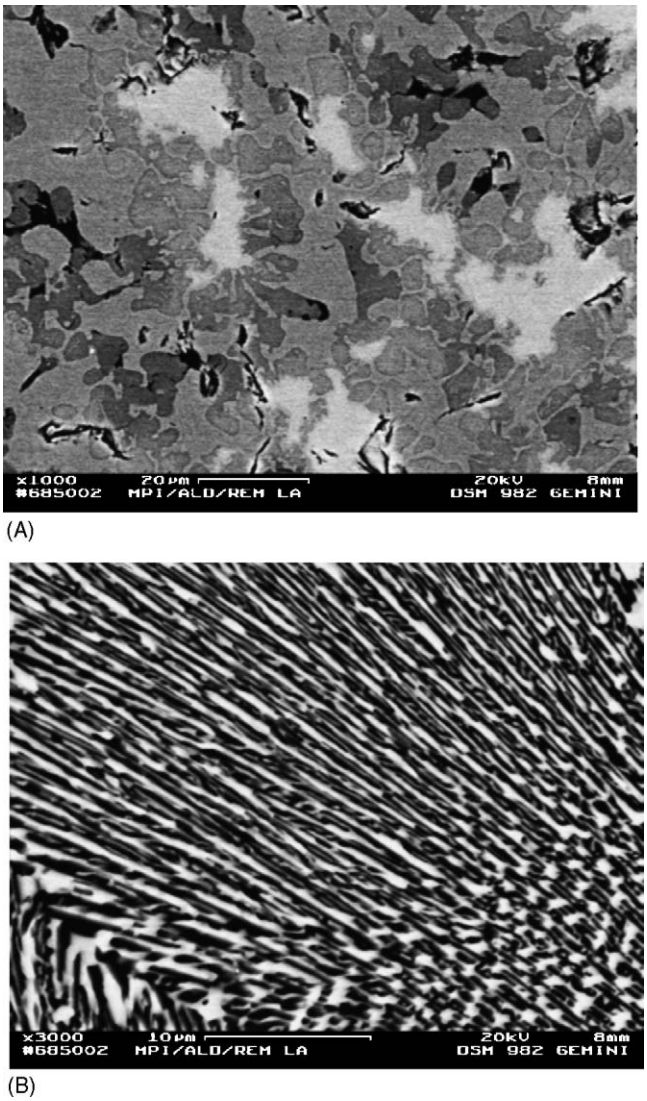


Fig. 5. Microstructures of some alloys in the system $Al_2O_3$–$ZrO_2$–$Nd_2O_3$, mol%. (A) Saddle point $23Al_2O_3$–$36ZrO_2$–$41Nd_2O_3$ ($e_5$): dark phase, F; grey phase, LA; white phase, $NZ_2$. (B) Ternary invariant point $53Al_2O_3$–$26ZrO_2$–$21Nd_2O_3$ ($E_2$): dark phase, β; grey phase, F; white phase, NA.

Table 1
Coordinates of experimentally determined and tentative invariant points in the $Al_2O_3$–$ZrO_2$–$Nd_2O_3$ system

| Equilibrium points | Temperature (°C) | Composition (mol%) | | | Invariant equilibrium |
|---|---|---|---|---|---|
| | | $Al_2O_3$ | $ZrO_2$ | $Nd_2O_3$ | |
| $U_1$ | 2040[a] | 7[a] | 17[a] | 76[a] | L + H ⇔ A + X |
| $e_5$ | 2030 | 23 | 36 | 41 | L ⇔ F + NA |
| $U_2$ | 2000[a] | 6 | 27 | 67 | L + X ⇔ A + F |
| $U_3$ | 1770 | 56 | 34 | 10 | L + T ⇔ AL + F |
| $E_1$ | 1750 | 19 | 21 | 60 | L ⇔ NA + F + A |
| $U_4$ | 1715 | 57 | 22 | 21 | L + AL ⇔ β + F |
| $E_2$ | 1675 | 53 | 26 | 21 | L ⇔ β + NA + F |

[a] Temperature and composition are shown tentatively.

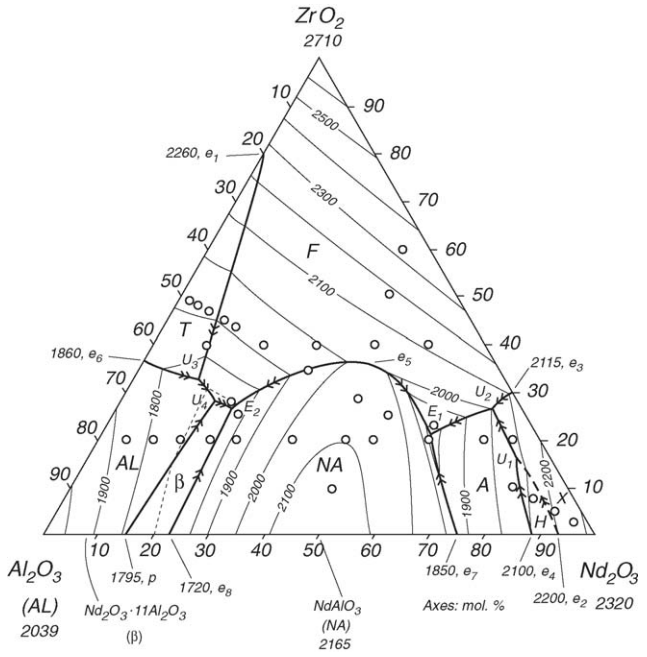


Fig. 6. Projection of the liquidus surface for the $Al_2O_3$–$ZrO_2$–$Nd_2O_3$ phase diagram.

## 2. Experimental details

Specimens were obtained by both chemical method and from melting the component oxides. Powders of alumina (99.9%), zirconia (99.99%), neodymia (99.9%) from Donetskij zavod khimreaktiviv, Donetsk, were used as raw materials. The appropriate quantities of oxides were blended in an agate mortar with ethanol, dried and pressed into pellets 5 mm in diameter and 5 mm in height.

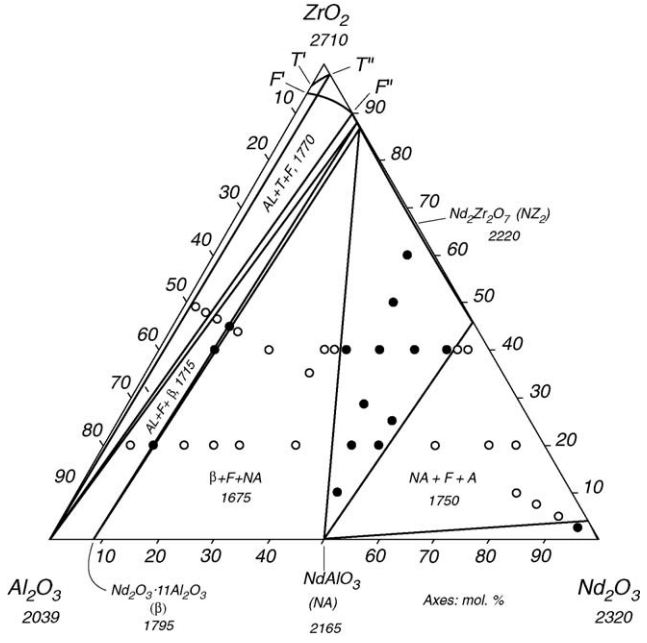


Fig. 7. Solidus surface projection for the $Al_2O_3$–$ZrO_2$–$Nd_2O_3$ phase diagram: (●) two-phase samples; (◯) three-phase samples.

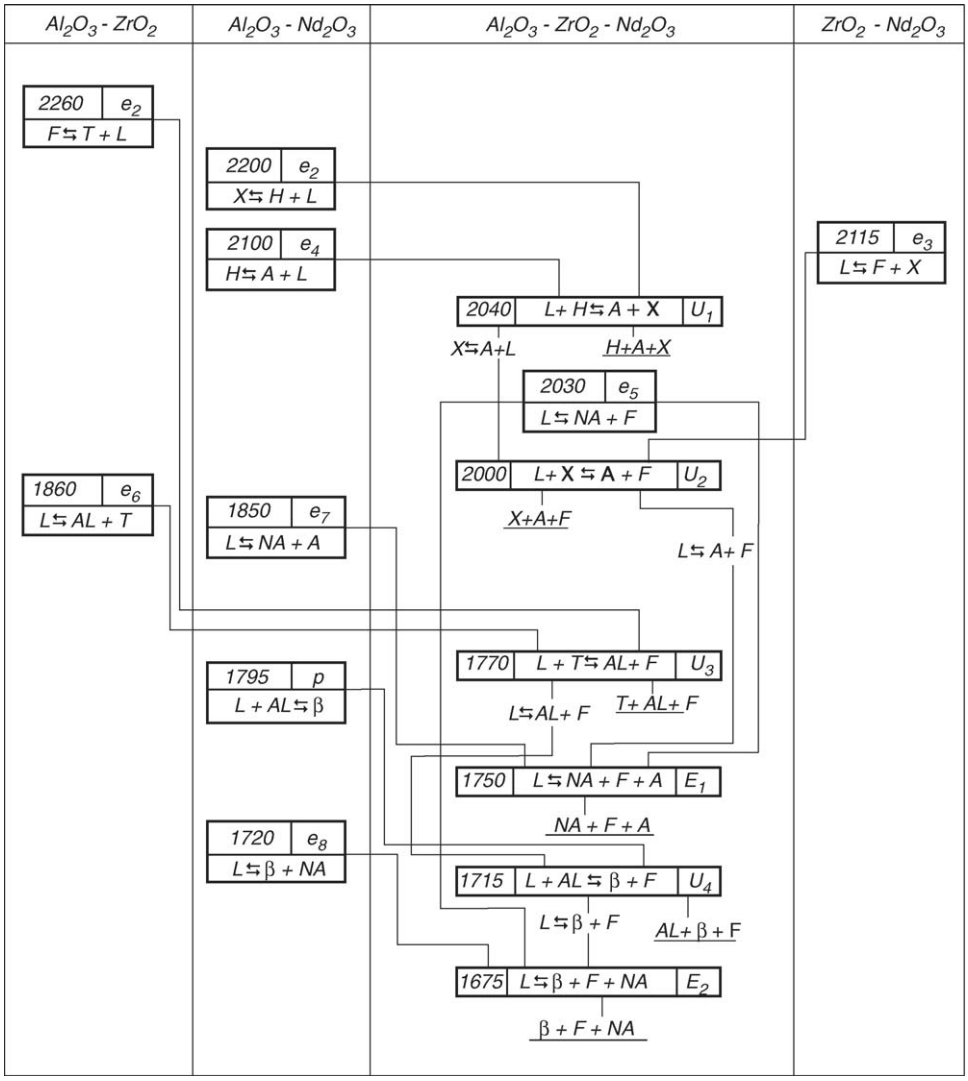


Fig. 8. Schematic of the reactions proceeding during sample crystallization in the $Al_2O_3$–$ZrO_2$–$Nd_2O_3$ system.

Powders of $Al(NO_3)_3{\cdot}9H_2O$, $ZrO(NO_3)_2{\cdot}2H_2O$ with purity 99.9% (Donetskij zavod khimreaktiviv, Donetsk) and neodymia (99.9%) were used for chemical route preparations. Both salts and neodymia were dissolved in water with some droplets of concentrated nitric acid added, dried, calcined at 900 °C in air and pressed into pellets of the same dimensions. The specimens were taken at 5–10 mol% intervals on the two isopleths: 20 and 40 mol% $ZrO_2$, on the bisector with a $Al_2O_3/ZrO_2$ ratio of 1, and along the section NA–(66.7% $ZrO_2$–33.3% $Nd_2O_3$). Additional compositions were chosen in the process of identifying the location of the ternary eutectic points. For the constructing of isothermal sections chemically derived samples were annealed at 1250 and 1650 °C for the time necessary to attain equilibrium, established by unchanging XRD patterns. Other samples were fired at 1250 °C in air for 6 h then melted in molybdenum pots in a DTA device[21] at total pressure of $H_2$ about 1.2 atm and annealed below the solidus temperature for 1 h. The specimens were investigated by X-ray (DRON-1,5, Burevestnik, St. Petersburg), DTA in $H_2$ at temperatures to 2300 °C,[21] petrographic (MIN-8 optical microscope, LOMO, St. Petersburg) and microstructure phase

Table 2
Coordinates of the apexes of the solid-phase tie-line triangles on the solidus surface of the $Al_2O_3$–$ZrO_2$–$Nd_2O_3$ phase diagram

| Phase field | Composition of the equilibrium phases (mol%) | | | | | |
|---|---|---|---|---|---|---|
| | AL | β | F | NA | A | T |
| AL + T + F | 100 | | 90 $ZrO_2$–10 $Nd_2O_3$ | | | 98.5 $ZrO_2$–1.5 $Nd_2O_3$ |
| AL + F + β | 100 | 100 | 88.5 $ZrO_2$–11.5 $Nd_2O_3$ | | | |
| β + F + NA | | 100 | 86.5 $ZrO_2$–13.5 $Nd_2O_3$ | 100 | | |
| NA + F + A | | | 46 $ZrO_2$–54 $Nd_2O_3$ | 100 | 4 $ZrO_2$–96 $Nd_2O_3$ | |

(ZEISS DSM982 GEMINI) analysis. The accuracy for XRD measurement came to ±0.0003 nm, for refractive indexes measured with immerse liquids ±0.003, with alloys—±0.02.

## 3. Results and discussion

Two isothermal sections at 1250 and 1650 °C were constructed incorporating literature data and the XRD results obtained (Figs. 2 and 3). No ternary compounds or regions of remarkable solid solutions were found in the components or binaries except small regions of ternary solid solutions in the $ZrO_2$ corners. They appeared because of limited $Al_2O_3$ and $Nd_2O_3$ solubility in $ZrO_2$ at elevated temperatures. Both isothermal sections are similar at $Nd_2O_3$ content less than 30 and more than 53%, the width of some regions changes because of their different extension in $ZrO_2$–$Nd_2O_3$ binary. The central parts of both sections are occupied by the equilibrium regions of NA with F and $NZ_2$ phases. At 1650 °C two-phase region NA + F edges the two- and three-phase areas, made by pyrochlore-like superstructure $NZ_2$ with F- and NA-phases. At 1250 °C the area of equilibrium of NA with F constricts owing to the eutectoid (1440 °C) decomposition of F-phase into $NZ_2$- and A-phase at the $Nd_2O_3$ content over ~40%.

The existence of two-phase regions NA + $NZ_2$, AL + F and β + F makes it possible to accept them as triangulating sections of the system $Al_2O_3$–$ZrO_2$–$Nd_2O_3$. As far as F and $NZ_2$ phases are of a variable composition and β-phase is stable only below 1795 °C[11] then these sections can be estimated as partially quasibinary. So as to estimating the $NZ_2$ entry mechanism into the system $Al_2O_3$–$ZrO_2$–$Nd_2O_3$ the polythermal (vertical) section NA–(66.7% $ZrO_2$–33.3% $Nd_2O_3$) was investigated (Fig. 4). The section is of the eutectic type and phase NA exhibits no solubility region. Solubility on the base of F and $NZ_2$ phases do not exceed 1 mol% at ambient temperature and slowly increases with temperature. The coordinate of the eutectic point was established as (mol%) 23$Al_2O_3$–36$ZrO_2$–41$Nd_2O_3$, 2030 °C (Fig. 5A). This eutectic point ($e_5$) is a saddle point in the phase diagram of the $Al_2O_3$–$ZrO_2$–$Nd_2O_3$ system (see Fig. 6) and was noted according to its temperature position in the ternary system. After alloys solidification the solid-phase transformation-ordering of

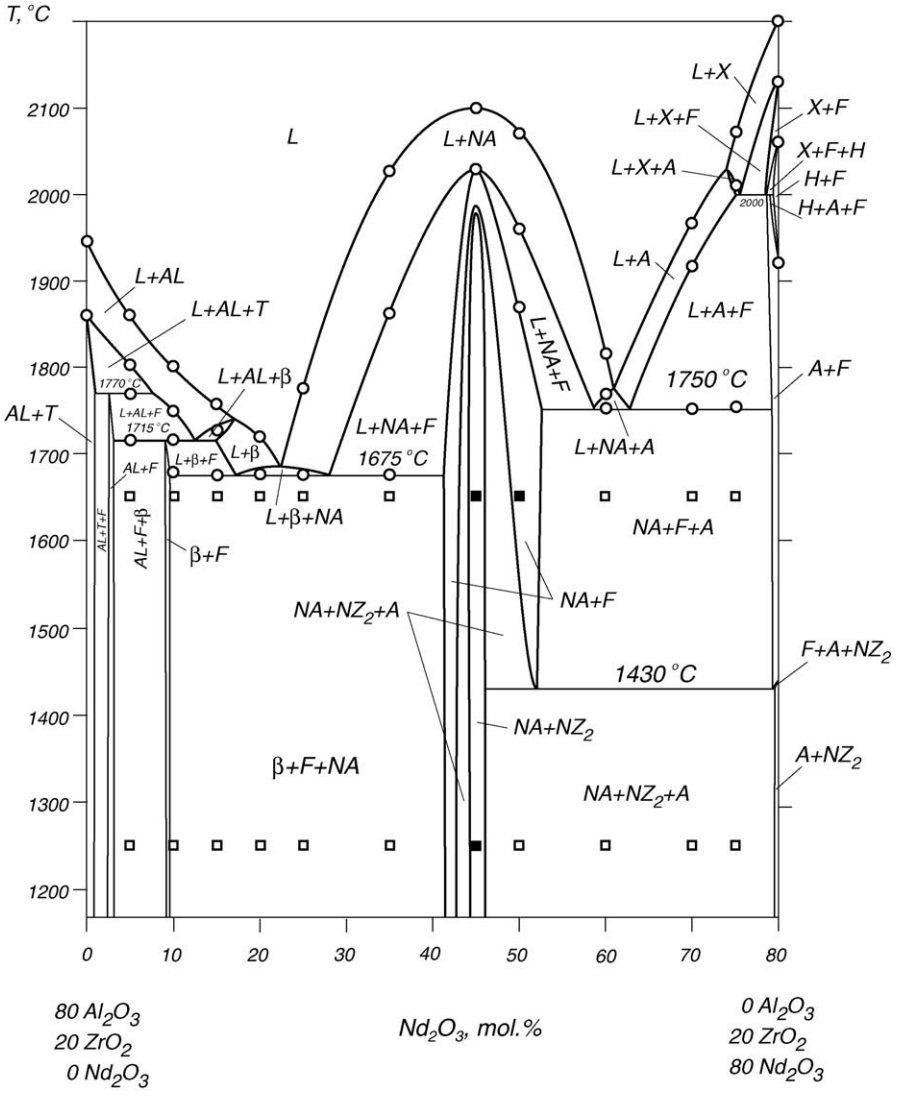


Fig. 9. Isopleth at 20 mol% $ZrO_2$ for the $Al_2O_3$–$ZrO_2$–$Nd_2O_3$ phase diagram.

the phase F into phase $NZ_2$ proceeds during some time and it is fixed in Fig. 5(A), where in the middle of the dark phase F appears light phase $NZ_2$.

The liquidus surface for the $Al_2O_3$–$ZrO_2$–$Nd_2O_3$ phase diagram (Fig. 6) consists of eight fields for primary crystallization. Every component and binary compound has its own field. No new phases or regions of remarkable solid solution were found in the components or binaries in the $Al_2O_3$–$ZrO_2$–$Nd_2O_3$ system. The largest liquidus area is occupied by solid solutions of $Nd_2O_3$ in $ZrO_2$. This field is divided by the monovariant line ($F \leftrightarrows T + L$) into two primary crystallization fields for solid solutions with fluorite-like cubic (F) and tetragonal (T) structures. The monoclinic form of $ZrO_2$ has no primary crystallization field on the liquidus because it exists at temperatures that do not exceed temperatures of binary and ternary eutectics. The $ZrO_2$ solid solutions in $Nd_2O_3$ with X- , H- and A-structures of rare-earth oxides have their own fields for primary crystallization. As far as high-temperature phases X and H cannot be quenched from high temperatures so the coordinates of monovariant curve $e_2U_1$ ($X \leftrightarrows H + L$) and nonvariant peritectic points $U_1$ and $U_3$ are shown tentatively. The coordinates of invariant points of the $Al_2O_3$–$ZrO_2$–$Nd_2O_3$ phase diagram are listed in Table 1. The microstructures of the invariant point $E_2$ is shown in Fig. 5(B). It should be noted that it was impossible to make a photo of ternary eutectic $E_1$ because of high hydration properties of $Nd_2O_3$ that was the component of this eutectic. The minimum melting temperature in the system is 1675 °C and relates to the ternary eutectic $E_2$. The maximum liquidus temperature is 2710 °C and refers to the melting point of pure $ZrO_2$.

The projection of the solidus surface of the $Al_2O_3$–$ZrO_2$–$Nd_2O_3$ phase diagram is shown in Fig. 7. Data on the coordinates of the conoid triangles of solid phases on the solidus surface were obtained from XRD measurements and are given in Table 2. According to the liquidus construction the solidus surface consists of six isothermal three-phase fields corresponding to two invariant equilibrium of the eutectic type and four of the peritectic type. The linear surfaces representing the solidification ends of the monovariant eutectics AL + T, AL + F, β + F, NA + F and NA + A are the parts of the solidus too. Two linear surfaces are also the solidus part: for the F solid solutions crystallization end, that is adjacent to the boundary system $ZrO_2$–$Nd_2O_3$ in the 10–54% $Nd_2O_3$ interval, and the linear surface F′T′F″T″ formed by the end of conoid triangles, which rest upon the equilibrium phases T and F whose compositions are located near the $ZrO_2$ apex and move upon curves T′T″ and F′F″. Two isothermal fields β + F + NA and NA + F + A that correspond to invariant eutectic equilibrium $L \leftrightarrows \beta + F + NA$ ($E_2$, 1675 °C)

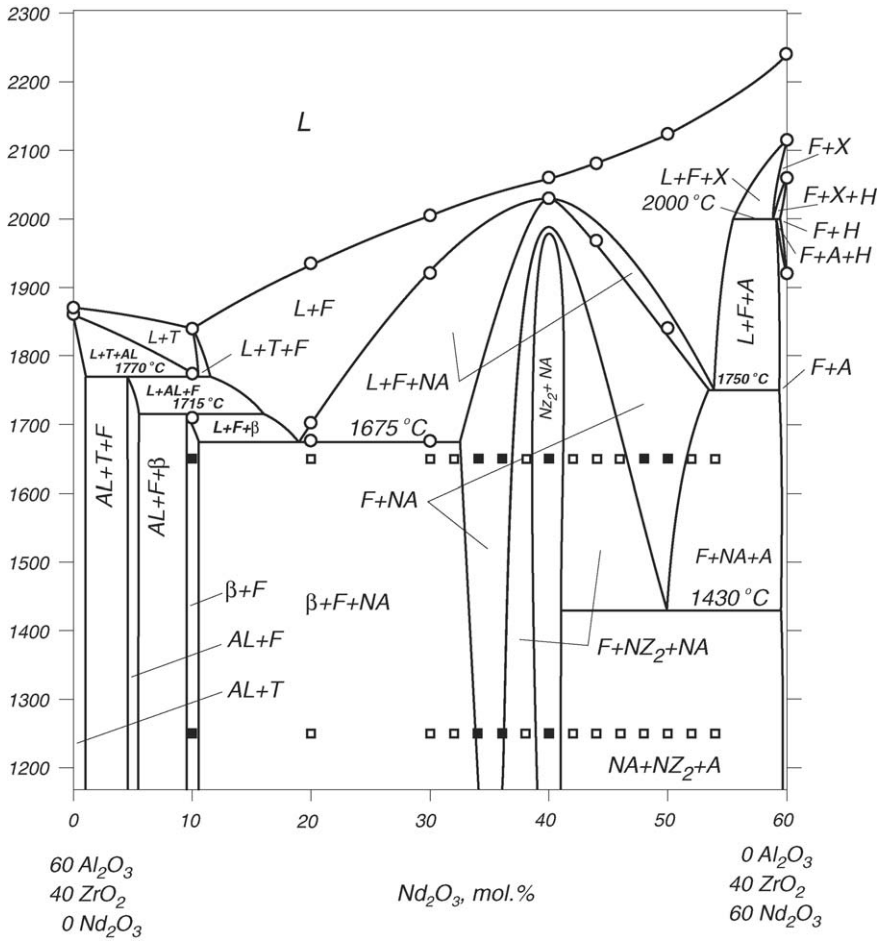


Fig. 10. Isopleth at 40 mol% $ZrO_2$ for the $Al_2O_3$–$ZrO_2$–$Nd_2O_3$ phase diagram.

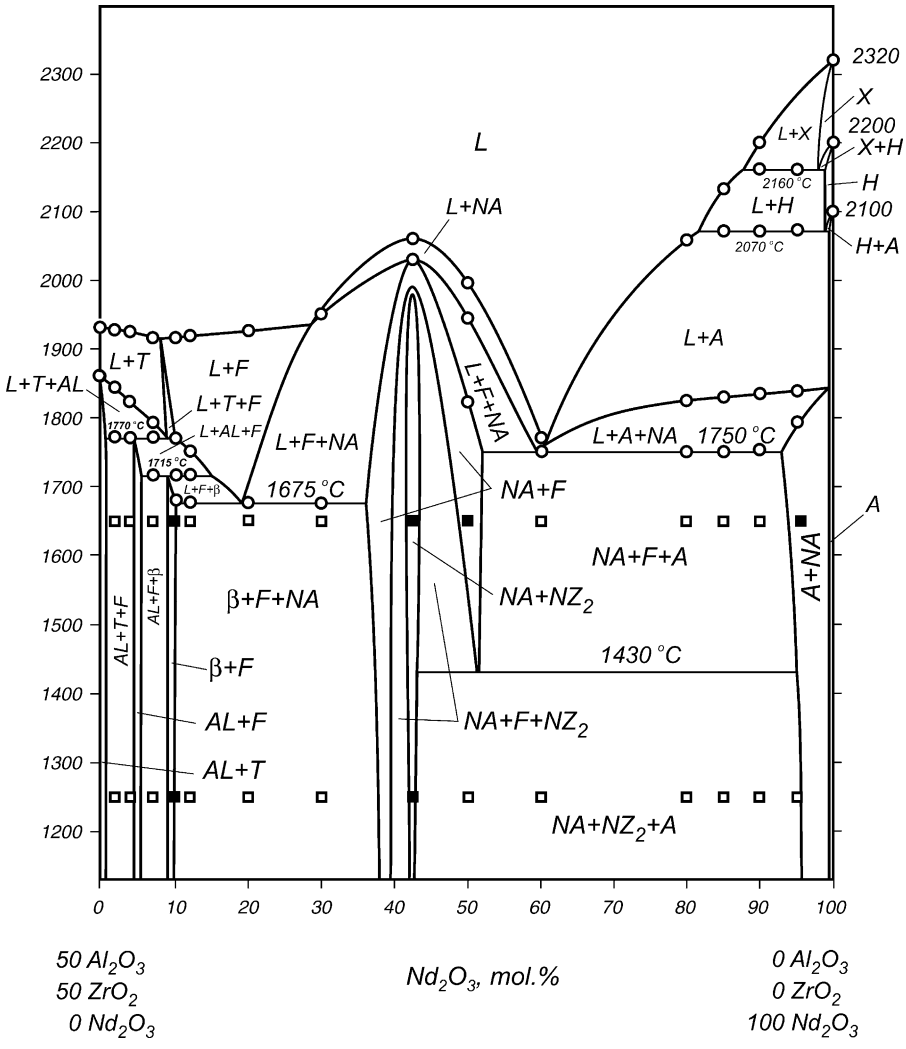


Fig. 11. Bisector $Al_2O_3/ZrO_2 = 1$ for the $Al_2O_3$–$ZrO_2$–$Nd_2O_3$ phase diagram.

and $L \leftrightarrows NA + F + A$ ($E_1$, 1750 °C), respectively, form the main solidus surface. Among four isothermal fields that correspond to invariant peritectic equilibria the largest ones are the fields AL + T + F and AL + F + β. They are the parts of peritectic quadrants, where the peritectic reactions $L + T \leftrightarrows AL + T$ ($U_3$, 1770 °C) and $L + AL \leftrightarrows \beta + F$ ($U_4$, 1715 °C) finish with total liquid expenditure. Other two isothermal fields of peritectic origin corresponding to phase transformations of $Nd_2O_3$ ($L + H \leftrightarrows A + X$, $U_1$, 2040 °C and $L + X \leftrightarrows A + F$, $U_2$, 2000 °C) are degenerated and located in the $Nd_2O_3$ corner.

On the base of data on liquidus, solidus and bounding binary systems a schematic of the reactions that proceed during the equilibrium crystallization of the $Al_2O_3$–$ZrO_2$–$Nd_2O_3$ system alloys is shown in Fig. 8. So the equilibrium alloys crystallization in this system is characterized with four invariant four-phase incongruent processes at 2040 ($U_1$), 2000 ($U_2$), 1770 ($U_3$), 1715 °C ($U_4$), two invariant four-phase congruent processes at 1750 ($E_1$) and 1675 °C ($E_2$) and one invariant three-phase congruent processes at 2030 °C ($e_5$) (Fig. 8).

Three polythermal sections were constructed to present the phase diagram of the $Al_2O_3$–$ZrO_2$–$Nd_2O_3$ system more completely: isopleths 20 and 40 mol% $ZrO_2$ and bisector $Al_2O_3/ZrO_2 = 1$ (Figs. 9–11). These figures confirm the triangulation and discover the interaction in different parts of the $Al_2O_3$–$ZrO_2$–$Nd_2O_3$ phase diagram.

## 4. Conclusions

The phase diagram of the $Al_2O_3$–$ZrO_2$–$Nd_2O_3$ system was constructed in the temperature range 1250–2800 °C. The liquidus surface of the phase diagram reflects the preferentially eutectic interaction in the system. Two new ternary and one new binary eutectics were found. The minimum melting temperature is 1675 °C and it corresponds to the ternary eutectic $Nd_2O_3 \cdot 11Al_2O_3$ + T-$ZrO_2$ + $NdAlO_3$. The solidus surface projection and the schematic of the alloy crystallization path confirm the preferentially congruent character of phase interaction in the ternary system. The polythermal sections present the complete phase diagram of the $Al_2O_3$–$ZrO_2$–$Nd_2O_3$ system. No ternary compounds or regions of remarkable solid solution were found in the components or binaries in this ternary system.

## References


1. Davtyan, I. A., Glushkova, V. B. and Keller, E. K., Investigation of the $ZrO_2$–$Nd_2O_3$ system. Zirconia-rich area investigation. *Izv. Akad. Nauk SSSR, Neorgan. Mater.*, 1965, **1**(5), 743–750.
2. Sakka, Y., Suzuki, T. S., Morita, K. and Hiraga, K., Colloidal processing and superplastic properties of fine-grained zirconia-based ceramics. *Key Eng. Mater.*, 2002, **206–213**, 645–648.
3. Gregorova, E., Havrda, J. and Pabst, W., ATZ ceramics prepared by slip-casting and centrifugal slip casting. *Key Eng. Mater.*, 2002, **206–213**, 369–372.
4. Rodriquez-Pulido, A., Ross, I. M. and Rainforth, W. M., Processing and structural characterisation of 3Y-TZP ceramics resistant to hydrothermal ageing. *Key Eng. Mater.*, 2002, **206–213**, 1053–1056.
5. Lakiza, S. M. and Lopato, L. M., Stable and metastable phase relations in the system Alumina–Zirconia–Yttria. *J. Am. Ceram. Soc.*, 1997, **80**(4), 893–902.
6. Bertaut, F. and Forrat, F., Etude des combinaisons des oxydes des terres rares avec l'alumine et la galline. *C. R. Acad. Sci. Paris*, 1956, **243**(17), 1219–1222.
7. Schneider, S. J., Roth, R. S. and Waring, J. L., Solid state reactions involving oxides of trivalent cations. *J. Res. Nat. Bur. Stand.*, 1961, **65A**(4), 345–374.
8. Toropov, N. A. and Kiseleva, T. P., The binary system neodymia–alumina and some data about the system neodymia–alumina–silica. *J. Neorgan. Chim.*, 1961, **6**(10), 2353–2358.
9. Godina, N. A. and Keller, E. K., Formation conditions of lanthanum, praseodymium and neodymium aluminates. *Izv. Akad. Nauk SSSR, Ser. Chim.*, 1966(1), 24–31.
10. Goldberg, D., Contribution a l'etude des systemes formes par l'alumine avec quelques oxydes de metaux trivalents et tetravalents, en particulier, l'oxyde de titane. *Rev. Int. Hautes Temp. Refract.*, 1968, **5**(3), 181–194.
11. Mizuno, M., Yamada, T. and Nogushi, T., Phase diagram of the system $Al_2O_3$–$Nd_2O_3$ at high temperatures. *J. Ceram. Soc. Jpn.*, 1977, **85**(2), 90–95.
12. Antic-Fidančhev, E. and Caro, P., Optical absorption spectrum of the β-alumina neodymia phase. *C. R. Hebd. Seances Acad. Sci., Ser. C*, 1977, **284**(13), 471–474.
13. Coutures, J. P., The $Al_2O_3$–$Nd_2O_3$ phase diagram. *J. Am. Ceram. Soc.*, 1986, **68**(3), 103–107.
14. Roth, R. S., Pyrochlore-type compounds containing double oxides of trivalent and tetravalent ions. *J. Res. Nat. Bur. Stand.*, 1956, **56**(1), 17–25.
15. Peres, Y. and Jorba, M., $ZrO_2$–rare earth oxides systems. *Ann. Chim.*, 1962, **7**(7–8), 479–511.
16. Rouanet, A., Contribution a l'etude des systemes zircone-oxydes des lanthanides au voisinage de la fusion. *Rev. Int. Hautes Temp. Refract.*, 1977, **8**(2), 161–180.
17. Zoz, H. I., Fomichov, E. N., Kalashnik, A. A. and Elisejeva, G. G., About the structure and properties of REE zirconates and hafnates. *J. Neorgan. Chim.*, 1982, **27**(1), 95–99.
18. Glushkova, V. B., Krzizanovskaya, V. К., Strahov, V. I., Sovestnova, O. A. and Novikov, V. К., Phase formation in the $ZrO_2$–$Nd_2O_3(Y_2O_3)$–$Al_2O_3(Cr_2O_3)$ systems and properties of based materials. *Ogneupori i Tehnicheskaya Keramika*, 2001(2), 16–21.
19. Red'ko, V. P., *Physico-chemical investigation of the compositions M4Zr(Hf)3O12 in the systems ZrO2(HfO2)–REE oxides*. Ph.D. theses, Frantsevich Institute for Materials Science Problems, Kyiv, Ukraine, 1990.
20. Lakiza, S. M. and Lopato, L. M., Phase diagram of the $Al_2O_3$–$ZrO_2$–$La_2O_3$ system. *J. Eur. Ceram. Soc.*, 2005, **25**(8), 1373–1380.
21. Lopato, L. M., Shevchenko, A. V. and Kuschevskij, A. E., Investigation of the refractory oxides systems. *Poroshkovaja Metallurgija*, 1972(1), 88–92.